The Scientific Temper
Vol. 17, No. 11, November 2026: pp. 7131-7143
ISSN: 0976-8653, E-ISSN: 2231-6396
DOI: 10.58414/SCIENTIFICTEMPER.2026.17.11.2580
A Web Of Science Journal

RESEARCH ARTICLE

Structural, Microstructural, and Lattice Strain Analysis of MgO Nanoparticles Synthesized by Chemical Co-precipitation

Sanchita De[1], and Baibaswata Bhattacharjee[2]*

*[*1]Department of Physics, Bankura Zilla Saradamani Mahila Mahavidyapith, Bankura-722101, India*

*[*2]Department of Physics, Ramananda College, Bishnupur, Bankura-722122, India*

***Corresponding author**: baib23@gmail.com*

ABSTRACT

Magnesium oxide (MgO) is a wide-bandgap ceramic dielectric material that has attracted considerable attention due to its promising potential in a wide range of industrial and technological applications. The chemical co-precipitation method was employed to synthesize MgO nanoparticles in this study. X-ray diffraction (XRD) analysis was carried out to examine the structural properties of the synthesized MgO nanoparticles. The average crystallite size was estimated to be between 14 and 25 nm using the Scherrer equation. Moreover, Williamson–Hall (W–H) analysis was used to assess the crystallite size along with the associated microstrain and residual stress. The morphological characteristics of the synthesized MgO nanoparticles were examined using scanning electron microscopy (SEM), which revealed a highly porous surface with irregularly shaped and agglomerated particles.

Keywords: *MgO nanoparticle, Chemical coprecipitation synthesis, Williamson-Hall analysis (UDM, UDSM, UDEDM).*

INTRODUCTION

Nanoparticles possess distinctive physicochemical properties arising from their nanoscale dimensions, size distribution, and morphology, which contribute to their broad applicability in advanced scientific and technological fields. Veerasamy, R et al. (2011). The synthesis method plays a crucial role in determining the size, shape, surface area, crystallinity, phase composition, and porosity of nanomaterials, which collectively influence their optical, electrical, magnetic, thermal, and catalytic properties. Varma, A. et al. (2016). Among the various synthesis techniques, the solution combustion method has emerged as an effective approach for producing nanoparticles with controlled particle size, high purity, and desirable morphological characteristics in a rapid and energy-efficient manner. Baiju, V. et al. (2021). Metal oxide nanomaterials possessing high surface area and porosity have attracted considerable research interest owing to their promising applications in nanoelectronics, optoelectronics, and sensing devices. Jintakosol, T. et al. (2009). Among the different metal oxide nanomaterials, magnesium oxide (MgO) stands out as an inorganic wide-bandgap ceramic dielectric material with significant potential for diverse industrial and technological applications. Amina, M. et al. (2020), Farhadi, S. et al. (2021), Wei, Q. et al. (2000). **Magnesium oxide (MgO)** is an alkaline earth metal oxide that crystallizes in a rock-salt (NaCl-type) cubic crystal structure. In its bulk form, MgO exhibits a wide band gap (approximately **7.3–7.8 eV**), high thermal conductivity, excellent chemical stability under dry atmospheric conditions, and a high melting

Received: 5th November, 2026 Accepted: 7th November, 2026 Published: 28th November, 2026

point (approximately **3125 K**), making it an important inorganic oxide for a wide range of technological applications. At the nanoscale, however, MgO displays significantly enhanced physicochemical properties owing to its reduced particle size, increased surface area, and the presence of structural defects. The large surface-to-volume ratio of MgO nanoparticles amplifies the influence of surface atoms, oxygen vacancies, undercoordinated ions, and lattice imperfections, leading to properties that differ markedly from those of bulk MgO. Furthermore, size-induced lattice strain and defect-related electronic states alter the optical, electronic, and catalytic characteristics of MgO nanoparticles. Consequently, nanostructured MgO may exhibit semiconductor-like optical behavior, making it highly attractive for advanced functional and optoelectronic applications. Hornak, J. et al. (2021) . Owing to its excellent physicochemical properties, MgO has been extensively utilized as a chemically stable buffer layer for high-temperature superconductors and ferroelectric thin films, a dielectric material in plasma display panels, and a low-loss dielectric component in microwave and high-capacity electronic devices. Additionally, MgO has demonstrated potential as an efficient catalyst support and gas scrubber for the removal of environmental pollutants, including CO_2, NO_x, and SO_x. Therefore, the synthesis of MgO nanoparticles with well-controlled structural integrity, strain characteristics, and morphology is of significant importance for tailoring their functional properties and expanding their advanced technological applications. Gatou, M.-A. et al. (2024).

EXPERIMENTAL METHODOLOGY

Material and Methods

In a typical synthesis procedure, 0.45 M magnesium nitrate hexahydrate ($Mg(NO_3)_2{\cdot}6H_2O$) (Sigma-Aldrich, purity 99.99%) was dissolved in 250 mL of distilled water and used as the precursor solution. A 0.65 M sodium hydroxide (NaOH) (Sigma-Aldrich, purity 99.99%) solution was added dropwise to the precursor solution under continuous stirring, resulting in the formation of a milky-white precipitate. The mixture was further agitated for an additional 30 min to ensure complete reaction. The obtained precipitate was collected, washed, and rinsed with methanol two to three times to remove residual ionic impurities. Subsequently, the precipitate was centrifuged at 3000 rpm for 10 min and dried at room temperature. The dried white powder samples were then calcined in air for 1 h at different temperatures (250, 350, 450, and 550 °C). The MgO nanoparticles calcined at 250, 350, 450, and 550 °C were designated as samples 1, 3, 4, and 6, respectively.The obtained powder samples were subsequently used for structural, morphological, and optical characterization.

Characterizations and Instrumentations

The structural characteristics of the synthesized samples were investigated using X-ray diffraction (XRD)(XRD, Bruker D8 Advance diffractomete), while their morphology and microstructural features were examined throughfield emission scanning electron microscopy (FESEM)(A Zeiss Sigma field emission scanning electron microscopy). The optical properties were evaluated using UV–Vis spectroscopy. The crystallite size, lattice strain, residual stress, and energy density were further analyzed using Williamson–Hall (W–H) methods based on the uniform deformation model (UDM), uniform stress deformation model (USDM), and uniform deformation energy density model (UDEDM). The results obtained from various characterization techniques were systematically correlated to establish the structure–property relationships of the synthesized MgO nanoparticles. ShunmugaSundaram, P. et al. (2020).

RESULTS AND DISCUSSION

XRD analysis

The XRD profile of the synthesized MgO nanoparticles showed the characteristic reflections of the MgO phase, confirming the successful synthesis and crystallization of MgO, as depicted in Fig. 1.

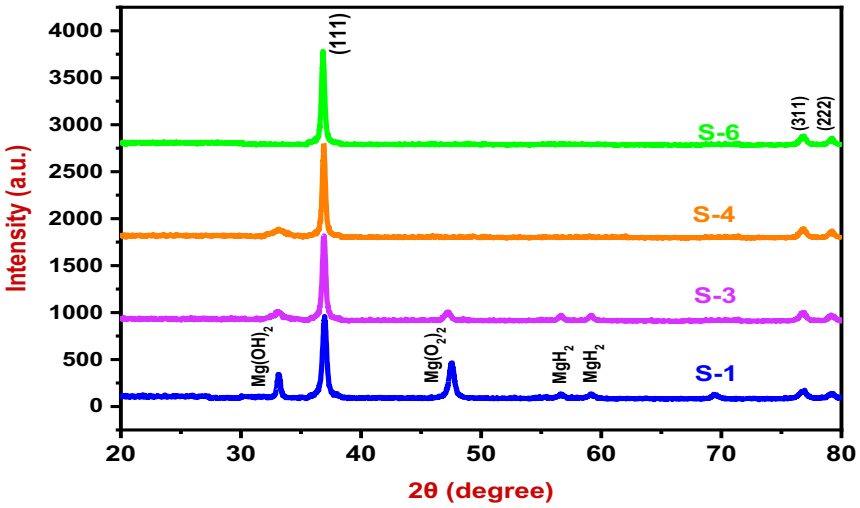

Fig 1. XRD profile of synthesized magnesium oxide (MgO) nanoparticles calcined at 250, 350, 450, and 550 °C

X-ray diffraction measurements were performed usingCu Kα radiation (λ = 1.5406 Å), and the diffraction patterns were recorded over a 2θ range of 20°–80°. The obtained XRD patterns revealed a cubic crystal structure of MgO, which was in good agreement with the standard JCPDS reference cards (Nos. 72-1427 and 36-1451), confirming the successful formation of MgO nanoparticles. Broadening of the XRD peaks can be attributed to the formation of MgOnanoparticles. The sample S-1 shows phases of $Mg(OH)_2$ and MgH_2 which are found to become weaker with increasing calcination temperature and consequently pure MgOphase is obtained after calcination of the samples at 350°C.

Table 1 presents a comparative analysis of the experimentally obtained 2θ values and interplanar spacing (d-values) with the corresponding JCPDS data for the identified crystal planes of the four samples. De, S. and Bhattacharjee, B. (2025).

The following formulae was employed to determine the lattice parameters of the crystal structure. Shaikh et al. (2022), Khorsand Zak et al. (2011).

$$\frac{1}{d^2} = \frac{h^2+k^2+l^2}{a^2} \quad (1)$$

In this expression, (d) represents the interplanar spacing, a denote the lattice constants, while (h), (k), and (l) correspond to the Miller indices. The value of (d) was calculated from Bragg's law. Shaikh et al. (2022), Khorsand Zak et al. (2011).

$$2dSin\theta = n\lambda \quad (2)$$

Once the lattice parameters a and d were determined, other structural parameters, such as the unit-cell volume ((VUC), atomic packing fraction (APF), and Mg–O bond length (BL), were calculated using Eqs. (3), (4), and (5), respectively. Javed et al. (2024), Shoeb et al. (2024).

$$V_{VUC} = a^3 \quad (3)$$

The atomic packing fraction (APF) is given by the following general expression:

$$APF = \frac{V_{ions}}{V_{unit\ cell}}$$

$$APF = \frac{16л(r^3_{Mg2+} + r^3_{O2-})}{3a^3} \quad (4)$$

Where, r_{Mg2+} =0.072 nm is ionic radius of the Mg^{2+} cation and r_{O2-} =0.140 nm is the ionic radius of the O^{2-} anion.

$$BL_{Mg-O} = \frac{a}{2} \quad (5)$$

The calculated structural parameters reveal that all MgO samples retain their characteristic cubic crystal structure. The slight variations in lattice parameter, unit-cell volume, atomic packing fraction, and Mg–O bond length among the samples can be attributed to the presence of lattice strain, structural defects, and nanoscale effects. The obtained Mg–O bond lengths are consistent with the MgO crystal structure, confirming the structural stability of the synthesized nanoparticles. Ceramurgia International (1979) . Increasing calcination temperature promotes removal of adsorbed species and structural relaxation, allowing the distorted lattice to become more relaxed. Changes in defect concentration, particularly oxygen-related defects, can also produce a small lattice expansion. Table-1 shows a gradual increase in 'a', for example approximately: 4.2066 to 4.22 A° with increasing calcination temperature. At lower calcination temperature, the nanoparticles contain relatively more lattice strain, defects and structural distortions. Hegde et al. (2024). With increasing temperature, atoms acquire sufficient thermal energy to rearrange toward more energetically stable positions and residual strain is relaxed. However, the final lattice parameter can increase slightly if the calcination-induced change in

defect chemistry-especially oxygen vacancies or other non-stoichiometric defects produces lattice expansion. With increasing calcination temperature, a gradual increase in the lattice parameter of the MgO nanoparticles was observed, accompanied by corresponding increases in the interplanar spacing, unit-cell volume, and Mg–O bond length. The increase in lattice parameter may be associated with thermally induced structural relaxation and changes in defect chemistry, particularly oxygen-related defects, within the MgO lattice. Since d, V_{VUC}, and Mg–O bond length are directly dependent on the lattice parameter, their increasing trends are consistent with the observed lattice expansion. In contrast, the atomic packing fraction decreases slightly with increasing calcination temperature because the increase in unit-cell volume is not accompanied by a proportional increase in the volume occupied by the constituent ions. Changes in oxygen-vacancy concentration or other defects can alter the local Mg–O coordination and produce a small expansion of the lattice. Rodenbough et al. (2017), Kaneko et al. (2010). The increase in the calculated Mg–O bond length with increasing calcination temperature suggests a slight expansion of the Mg–O interionic separation, consistent with the observed increase in lattice parameter. This variation may be associated with thermally induced lattice relaxation and changes in the defect environment of the MgO nanoparticles.

With increasing calcination temperature from 250°C to 550°C, the most intense XRD diffraction peak shifts slightly toward lower 2θ angles, from 36.9654° to 36.8222° (Fig. 2)(value taken from Gauss fit data). According to Bragg's law, this shift corresponds to an increase in interplanar spacing. The observed shift may be associated with changes in lattice parameters, residual strain, and defect concentrations in MgO nanoparticles. Meanwhile, the decreasing FWHM ($FWHM_{S-1}$ = 0.30291, $FWHM_{S-3}$= 0.28541, $FWHM_{S-4}$= 0.242, $FWHM_{S-6}$= 0.2358) suggests a reduction in diffraction peak broadening, which may be attributed to crystallite growth and the relaxation of lattice strain at higher calcination temperatures. Hassanzadeh-Tabrizi, S. A. et al. (2023). These results indicate temperature-dependent changes in the structural properties of the synthesized MgO nanoparticles. The increase in XRD peak intensity with increasing calcination temperature may be attributed to enhanced crystalline ordering and crystallite growth. The accompanying decrease in FWHM suggests reduced diffraction peak broadening, potentially due to an increase in coherent crystallite size and a reduction in microstrain. These observations indicate temperature-dependent changes in the structural characteristics of the MgO nanoparticles. Nevertheless, changes in preferred orientation and experimental conditions should also be considered when interpreting variations in diffraction intensity. Gopinath Kasi et al. (2025).

Table 1: Comparison of 2θ, 'a' and 'd' values of MgO Samples

S - 1	2θ	36.9654	76.807	79.2066
	d spacing (A°)	2.4298	1.24	1.2084
	Lattice parameter (a)	4.2086	4.1127	4.1859
	Unit-cell volume $(A°)^3$	74.5432	69.5638	73.3459
	Atomic packing fraction (%)	70.0311	75.0440	71.17 43
	Bond length (A°)	2.1043	2.0564	2.0930
S - 3	2θ	36.904	76.801	79.1803
	d spacing (A°)	2.4324	1.2401	1.2087
	Lattice parameter (a)	4.2131	4.113	4.1871
	Unit-cell volume $(A°)^3$	74.7826	69.5776	73.4069
	Atomic packing fraction (%)	69.8070	75.0291	71.1152
	Bond length (A°)	2.1065	2.0564	2.0935
S - 4	2θ	36.8836	76.7894	79.16929
	d spacing (A°)	2.435	1.2403	1.209
	Lattice parameter (a)	4.2176	4.1135	4.1876
	Unit-cell volume $(A°)^3$	75.0229	69.6042	73.4325
	Atomic packing fraction (%)	69.5833	75.0005	71.0904
	Bond length (A°)	2.1087	2.0567	2.0937
S - 6	2θ	36.8222	76.6979	79.0566
	d spacing (A°)	2.4389	1.2415	1.2103
	Lattice parameter (a)	4.2244	4.1176	4.1926
	Unit-cell volume $(A°)^3$	75.3858	69.8149	73.6952
	Atomic packing fraction (%)	69.2485	74.7741	70.8370
	Bond length (A°)	2.1122	2.0588	2.0963
hkl		111	311	222

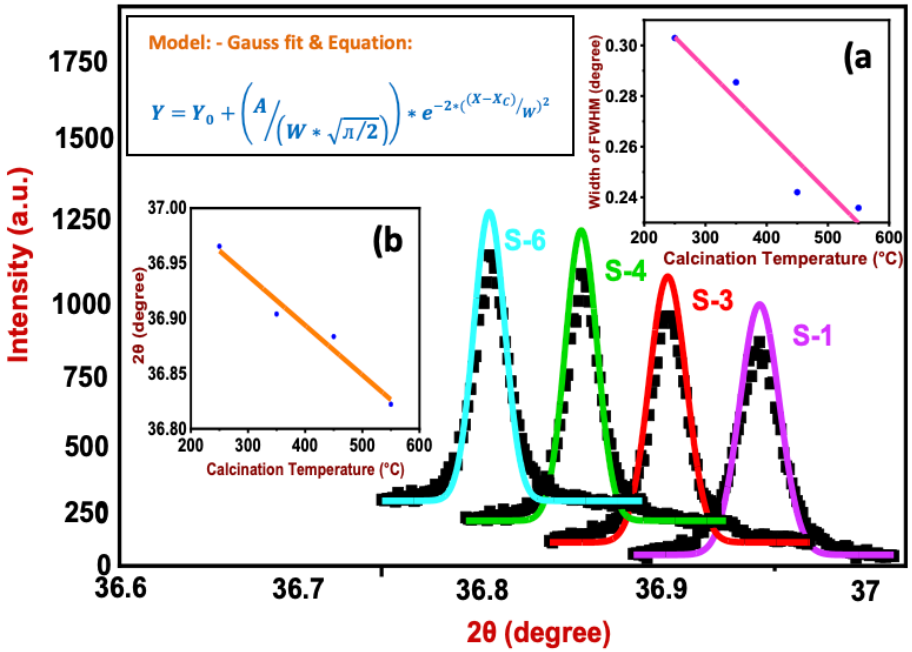

Fig 2. Variation of FWHM of different samples. (a) Variation of FWHM with calcinations temperature. (b) Variation of 2θ (degree) with calcination temperature.

Crystallite Size Estimation Using the Scherrer Equation

Table 2 presents the crystallite sizes of the synthesized MgO nanoparticles calculated using the Scherrer equation. The diffraction angle (2θ) and full width at half maximum (FWHM) values were obtained from the XRD patterns. The average crystallite size (D) was estimated using the Scherrer equation based on the observed peak broadening. Jensen, H. et al. (2006). The full width at half maximum (FWHM) values of the prominent diffraction peaks were obtained through nonlinear curve fitting using a Gaussian function. These values were subsequently used to estimate the crystallite size of the synthesized MgO nanoparticles using the Scherrer equation. The calculated crystallite sizes are summarized in Tables 2 . The Miller indices and lattice parameters were determined from the experimentally obtained interplanar spacing (d-values), and the results were found to be in good agreement with the corresponding values reported in the JCPDS database. Dislocation density (δ) is a key structural parameter that provides an estimation of the defect density in MgO samples. It quantifies the total dislocation length present within a unit volume of the crystal lattice and is expressed in lines per square meter (m^{-2}). The corresponding relationship for calculating dislocation density is given as follows.

$$\delta = \frac{1}{D^2} \quad (6)$$

where **D** represents the calculated crystallite size of the MgO nanoparticles. N.

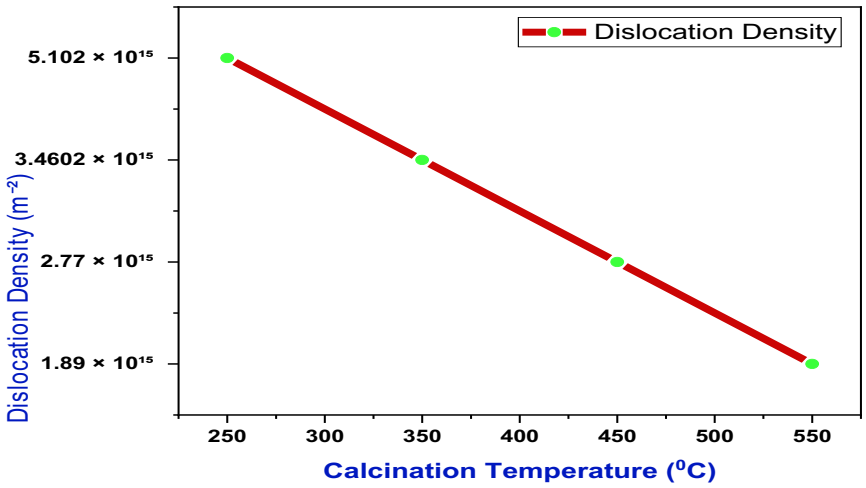

Fig 3. Variation of dislocation density with calcination temperature of magnesium oxide (MgO) nps.

Table 2: The average crystallite size of the synthesized MgO nanoparticles was estimated using the Scherrer equation based on the XRD peak broadening

Sample Code	βcosθ	D(nm)	δ (m^{-2})
S - 1	0.0103	15	5.102×10^{15}
S - 3	0.009	17	3.4602×10^{15}
S - 4	0.0074	20	2.77×10^{15}
S - 6	0.0062	24	1.89×10^{15}

Rani et al. (2019). The dislocation density values calculated from the crystallite sizes obtained through the Scherrer equation, nonlinear curve fitting, and XRD measurements were found to be 5.102×10^{15} m^{-2}, 3.4602×10^{15} m^{-2}, 2.77×10^{15} m^{-2}, and 1.89×10^{15} m^{-2}, respectively. The relatively low dislocation density indicates a lower concentration of crystallographic defects, suggesting improved structural integrity and larger crystallite dimensions. These results imply that, despite the presence of lattice strain, the crystalline quality of the MgO nanoparticles remains largely preserved. The estimation assumes a uniform distribution of dislocations within the crystallites, with the crystallite size determined from XRD analysis exhibiting an inverse relationship with dislocation density. Furthermore, the dislocation density decreases with increasing calcination temperature, indicating enhanced crystallinity at higher annealing temperatures.

Williamson–Hall method

Model based on Uniform Deformation(UDM)

The Uniform Deformation Model (UDM), a simplified approach based on the Williamson–Hall (W–H) method, assumes isotropic microstrain and enables a rapid estimation of crystallite size and lattice strain from multiple XRD reflections. Wadhwa, S. et al. (2019), Kumar, S.A. et al. (2022). The strain present in the synthesized powders, originating from lattice distortions and crystalline defects, was calculated using Eq. (7). The corresponding Williamson–Hall equation based on the UDM approach is expressed in Eq. (8).

$$\varepsilon = {}^{\beta}/_{4\tan\theta} \quad (7)$$

$$\beta \cos\theta = {}^{Q\lambda}/_{D} + 4\varepsilon \sin\theta \quad (8)$$

According to the Uniform Deformation Model (UDM), the material is assumed to exhibit isotropic deformation, where the strain is independent of crystallographic direction. The crystallite size (D) and microstrain (ε) were determined from the Williamson–Hall plot, as shown in Fig. 3. The slope of the linear fitting corresponds to the microstrain, while the y-intercept provides the value of Qλ/D, which is related to the crystallite size. Figure 3 illustrates the 4sinθ versus βcosθ plot for MgO nanoparticles, with the calculated strain and crystallite size values obtained from the linear fitting.

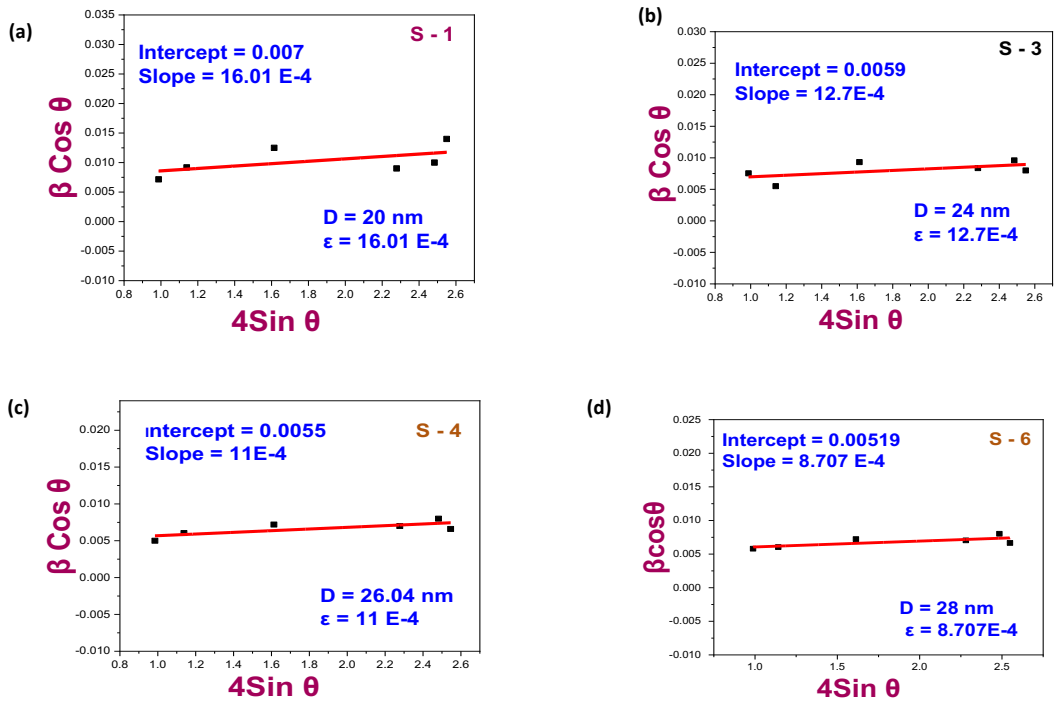

Fig. 4. (a) – (d)4sinθ vs. βcosθ plot of S–1,S-3,S-4,S-6

Model based on Uniform Deformation Stress(UDSM)

The Uniform Stress Deformation Model (USDM) is an extended form of the Williamson–Hall (W–H) analysis, which is employed to estimate microstrain, crystallite size, and residual stress in crystalline materials using XRD data. Wadhwa, S. et al. (2019), Kumar, S.A. et al. (2022). Unlike the simpler Uniform Deformation Model (UDM), which assumes uniform strain distribution, the USDM considers the elastic properties of the material through Young's modulus (E) to establish the relationship between strain and residual stress (σ). The Uniform Stress Deformation Model (USDM) can be considered an extension of the Uniform Deformation Model (UDM) by incorporating the mechanical properties of the material. According to Hooke's law, within the elastic deformation region and at very low strain levels, stress (σ) exhibits a linear relationship with strain (ε). Wang, Y. et al. (2008). Assuming the presence of small strains in the synthesized MgO nanoparticles, the Williamson–Hall equation can be modified by incorporating Hooke's law, resulting in the USDM expression, which is represented by Eq. (9).

$$\beta \cos\theta = \left({}^{Q\lambda}/_{D}\right) + {}^{4\varepsilon \sin\theta}/_{E} \qquad (9)$$

The Young's modulus of MgO nanoparticles may vary depending on the material system, synthesis route, and structural characteristics, with reported values typically ranging from approximately 13.9 to 248.73 GPa. By plotting 4sinθ/E along the x-axis against βcosθ along the y-axis, the residual stress (σ) and crystallite size (D) can be determined from the slope and y-intercept of the linear fit, respectively. For cubic crystalline materials, the elastic modulus parameter can be estimated using the following equation (Eq. 10).

$${}^{1}/_{E} = Z_{11} + 2(Z_{11} - Z_{12} - 0.5Z_{44})\,(q_1^2q_2^2 + q_2^2q_3^2 + q_1^2q_3^2) \qquad (10)$$

Where $Z_{ij}$are elastic compliance (for cubic MgO, Z_{11} =4.01 TPa^{-1}, Z_{12} =6.46 TPa^{-1}, and Z_{44} = 0.96 TPa^{-1}, whereas

$$q_1 = h(h^2 + k^2 + l^2)^{-1/2}$$

$$q_2 = k(h^2 + k^2 + l^2)^{-1/2}$$

$$q_3 = l(h^2 + k^2 + l^2)^{-1/2}$$

The Young's modulus (E) of the MgO nanopowders was determined to be 309.33 GPa, and the corresponding elastic modulus values obtained for all samples are presented in Table 3

Table 3: Elastic modulus values for all samples of MgO nanoparticle

Sample Code	E (GPa)
S-1	350
S-3	320
S - 4	270

The stress values determined through this model represent internal residual stresses rather than externally applied mechanical loads. These residual stresses may originate from factors such as lattice mismatch, surface tension effects, crystallographic defects, and non-uniform cooling during synthesis or processing. The stress values obtained from the USDM analysis are presented in Fig. 4. The corresponding strain values were estimated to be 18.13×10^{-4}, 12.45×10^{-4}, 9.25×10^{-4} and 7.27×10^{-4} for samples S-1, S-3, S-4, and S-6 respectively.

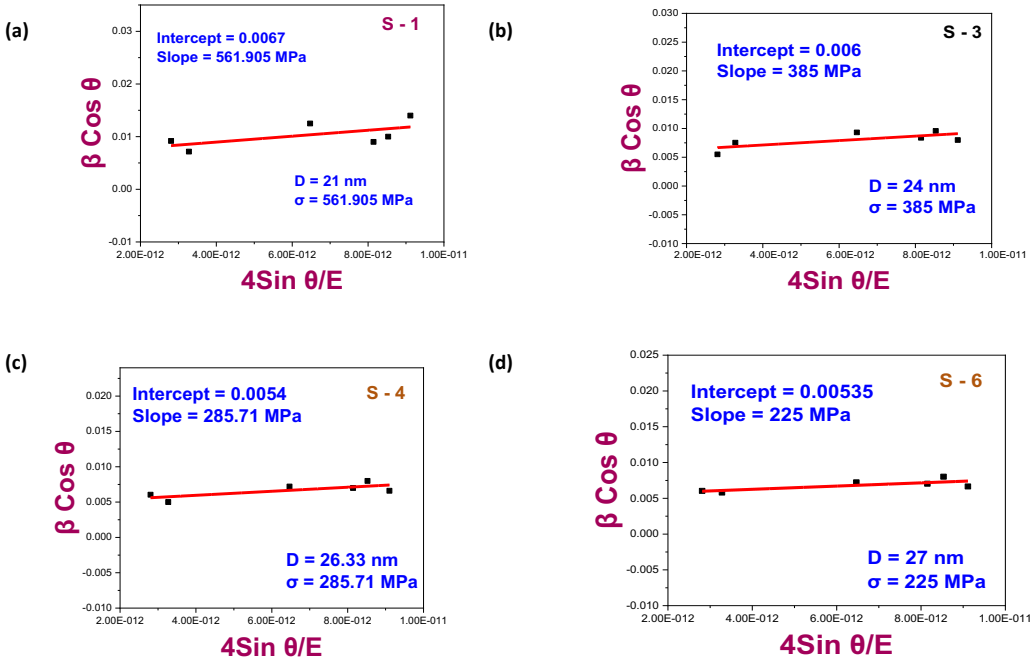

Fig. 5. (a) – (d) 4sinθ / E vs. βcosθ plot of S–1, S-3, S-4 & S-6

Model based on Uniform Deformation Energy Density (UDEDM)

The Uniform Deformation Energy Density Model (UDEDM) represents a further extension of the Williamson–Hall (W–H) approach and is employed in XRD line profile analysis to determine the crystallite size (D), microstrain (ε), and elastic strain energy density (u) associated with lattice distortions. Wadhwa, S. et al. (2019), Kumar, S.A. et al. (2022). Unlike the conventional W–H models, the UDEDM considers the contribution of strain energy density, where the proportionality constants related to the strain–stress relationship are influenced by the stored elastic energy within the crystal lattice. According to Hooke's law, the elastic strain energy density can be expressed as $u=\varepsilon^2E/2$. By incorporating this relationship into the Williamson–Hall equation, the modified W–H expression based on the UDEDM approach can be obtained as follows:

$$\beta \cos\theta = \left(\frac{Q\lambda}{D}\right) + 4\varepsilon \sin\theta \left(\frac{2u}{E}\right)^{1/2} \qquad (11)$$

The UDEDM analysis was performed by plotting $4\sin\theta(2/E)^{1/2}$ as a function of βcosθ. The slope obtained from the linear regression represents $u^{1/2}$, whereas the y-intercept is used to determine the crystallite size (D) of the synthesized MgO nanoparticles. Figure 5 illustrates the 4sinθ sqrt(2/E) versus βcosθ plot for MgO nanoparticles based on the UDEDM analysis. Using the relationships $u=\varepsilon^2E/2$ and $\sigma=E\varepsilon$ derived from Hooke's law, the correlation between the elastic strain energy density (u) and residual stress (σ) can be expressed as $u=\sigma^2/2E$.Furthermore, the lattice strain was evaluated using the Young's modulus (E) of the MgO specimens. The strain values obtained from the UDEDM analysis were found to be 16.9×10^{-4}, 11.2×10^{-4}, 11.01×10^{-4}, and 8.8×10^{-4}, while the corresponding residual stress values were estimated as 591 MPa, 357.76 MPa, 288.6 MPa, and 227.156 MPa for samples S-1, S-3, S-4, and S-6, respectively.

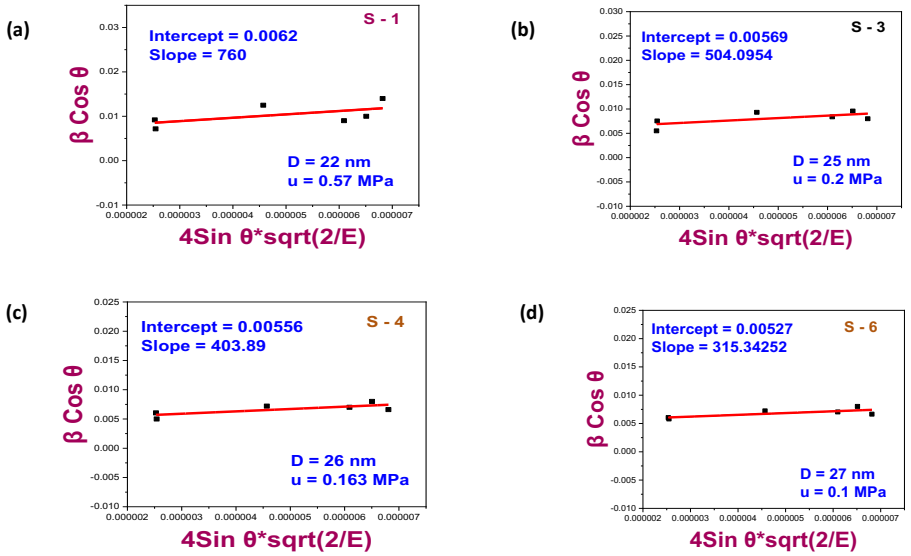

Fig. 6. (a) – (d) 4sinθ sqrt (2/E) vs. βcosθ plot of S–1, S-3, S-4 & S-6

Table 4 summarizes the crystallite sizes of the MgO nanoparticles synthesized in this study, as determined using the Scherrer equation and various Williamson–Hall models. The comparison of stress and strain values obtained from different models is presented in Table 5. MgO nanoparticles generally exhibit lower elastic constants compared with their bulk counterparts due to nanoscale effects, including increased surface area, size-dependent structural changes, and defect concentration. However, the specific elastic properties may vary considerably depending on the synthesis conditions and the resulting microstructural characteristics of the nanomaterials. Theoretical calculations and experimental investigations are essential for understanding the elastic properties of MgO nanoparticles under different conditions. The slight variation in crystallite size values obtained from the Scherrer equation and Williamson–Hall (W–H) analysis may be attributed to differences in the underlying assumptions of these methods and the averaging effect of particle size distribution.The Scherrer equation attributes XRD peak broadening exclusively to finite crystallite size, whereas the Williamson–Hall (W–H) method separates the contributions of crystallite size and lattice strain to the observed peak broadening. Since the lattice strain present in the synthesized MgO nanoparticles is relatively low, both approaches yield comparable crystallite size values, with minor variations arising from the strain effects considered in the W–H analysis.

Table 4: Crystallite sizes from Scherrer equation and other models of WH method

Sample Code	Scherrer Equation	UDM	USDM	UDEDM
S-1	15	20.68	21.61	21.87
S-3	17	24.5	24.13	25
S-4	20	26.04	26.33	26
S-6	24	27.9	27.06	27.47

Table 5: Stress-Strain value comparison obtained from different models

Sample Code	UDM	USDM		UDEDM		
	Strain	Stress(MPa)	Strain	Stress(MPa)	Strain	Energy Density(MPa)
S-1	$16x10^{-4}$	561	$18.13x10^{-4}$	591	$16.9x10^{-4}$	0.5776
S-3	$12x10^{-4}$	385	$12.45x10^{-4}$	357.76	$11.18x10^{-4}$	0.254
S-4	$11x10^{-4}$	285.71	$9.25x10^{-4}$	288.6	$11.01x10^{4}$	0.163
S-6	$8.707x10^{-4}$	225	$7.27x10^{-4}$	227.156	$8.8x10^{-4}$	0.1

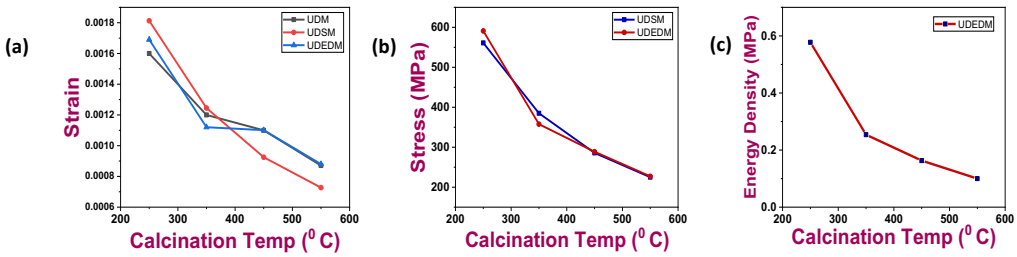

Fig. 7. (a) Variatioof Strain with Calcination Temperature for UDM, UDSM& UDEDM model (b) Variatio of Stress with Calcination Temperature for UDSM& UDEDM model (c) Variatio of energy densit with Calcination Temperature for UDEDM model.

The variations in crystallite size and strain obtained from different W–H models indicate the influence of residual stress and strain energy density on lattice deformation. The USDM and UDEDM approaches provide a more comprehensive description of strain distribution in MgO nanoparticles compared with the simplified uniform strain assumption of the UDM.

The lower lattice strain obtained from the UDSM compared to the UDM and UDEDM at higher calcination temperatures is attributed to the incorporation of the crystallographic Young's modulus in the UDSM analysis. Unlike the UDM, which assumes that all peak broadening originates from uniform strain, the UDSM separates the contribution of elastic stress using Hooke's law. Furthermore, higher calcination temperatures enhance crystallinity, promote grain growth, and reduce lattice defects and residual stresses, resulting in a significant decrease in elastic deformation. Therefore, the UDSM provides lower and more realistic microstrain values than the UDM and UDEDM for well-crystallized MgO nanoparticles.The stress estimated using the Uniform Stress Deformation Model (USDM) is lower than that obtained from the Uniform Deformation Energy Density Model (UDEDM) at higher calcination temperatures because thermal treatment reduces lattice defects and residual microstrain, resulting in stress relaxation. However, UDEDM accounts for the elastic deformation energy stored within the crystal lattice, making it more sensitive to the remaining strain energy associated with grain boundaries and lattice imperfections. Consequently, UDEDM generally predicts higher stress values than USDM for MgO nanoparticles at elevated calcination temperatures.The deformation energy density of MgO nanoparticles decreases with increasing calcination temperature because thermal treatment enhances crystallinity, promotes grain growth, and reduces lattice defects and microstrain. As a result, residual internal stress is relieved and less elastic energy is stored in the crystal lattice. Since the deformation energy density in the UDEDM is proportional to the square of the lattice strain $u=Y\varepsilon^2/2$, the reduction in microstrain at higher calcination temperatures causes a significant decrease in the calculated energy density.

The higher stress, strain, and energy density observed in the MgO nanoparticles calcined at lower temperatures may be associated with their smaller crystallite size and higher concentration of lattice defects. Hegde, V. N., et al. (2024), RSC Advances (2015). particularly oxygen vacancies. At relatively low calcination temperatures, incomplete lattice rearrangement can result in a greater concentration of oxygen-deficient sites. The removal or loss of O^{2-} ions from the MgO lattice can create oxygen vacancies and locally disturb the Mg–O coordination environment. Rani, N., Chahal et al. (2019). Thereby inducing lattice distortion and internal stress. The higher density of such defect sites in smaller crystallites can consequently contribute to enhanced microstrain and elastic strain-energy density. With increasing calcination temperature, enhanced atomic diffusion and lattice rearrangement promote crystallite growth and structural relaxation. Scientific Reports (2026). resulting in a reduction in defect-related lattice distortion and, consequently, lower stress, strain, and energy density.

SEM analysis

Figure 8 presents the SEMimages of the synthesized MgO nanoparticles recorded at different magnifications. The images reveal the formation of large-scale flower-like hierarchical structures, which are attributed to the aggregation and self-assembly of thin sheet-like particles. M. Chen et al. (2017). These thin sheets undergo aggregation and interconnection, forming a three-dimensional network of flower-like MgO structures. This hierarchical architecture generates large pores, which can enhance the absorption mechanism by providing improved accessibility to internal surface-active sites. S. Ahmed et al. (2021). Although the particles appear to be in close contact with each other, no strong interparticle bonding is observed, allowing individual particles to maintain their distinct morphology, characteristics, and structural features. The particles primarily undergo physical aggregation, where they cluster together without the formation of chemical bonds. The average nanoparticle size was estimated using ImageJ software, and the calculated particle size was found to be in the range of 15–30 nm.

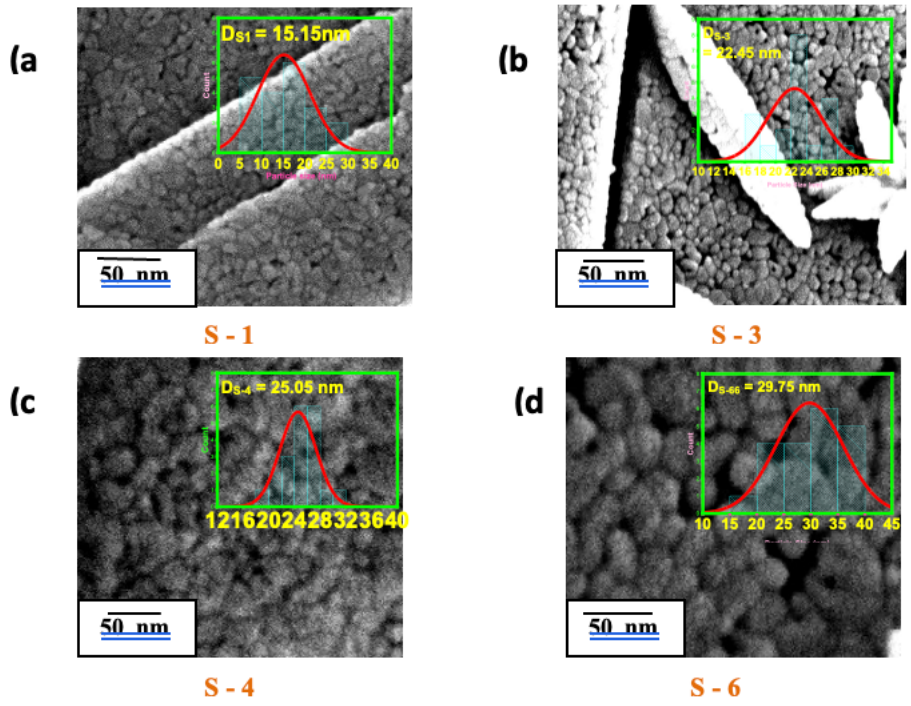

Fig. 8. SEM Image of (a) S-1 (b) S-3 (c) S-4 (d) S-6 MgO Nanoparticles at 50 nm magnification.

CONCLUSION

Comprehensive structural characterization of the synthesized MgO nanoparticles using XRD coupled with Williamson–Hall analysis models (UDM, USDM, and UDEDM) provided valuable insights into crystallite size, microstrain, and dislocation density, revealing the good structural integrity and crystalline quality of the nanoparticles. The XRD investigation indicated an average crystallite size of 14–24 nm for the synthesized MgO nanoparticles. Further evaluation using different Williamson–Hall models showed that the crystallite sizes were estimated to be 20–28 nm using UDM, 21–27 nm using USDM, and 22–27 nm using UDEDM, demonstrating slight variations due to the different assumptions incorporated in each model. The stress–strain evaluation demonstrated that the MgO nanoparticles possess microstrain values in the range of 10^{-4}, accompanied by associated stress and strain energy density, confirming the occurrence of lattice distortions arising from structural imperfections.The observed microstructural features have a crucial impact on the structural stability, optical properties, and surface activity of MgO nanoparticles, highlighting their significance for both fundamental investigations and technological applications .UDM assumes isotropic and uniform lattice strain. Since MgO nanoparticles may possess crystallographic defects and anisotropic deformation, UDSM was used to incorporate the directional Young's modulus and estimate the corresponding deformation stress.UDSM is based on a linear stress–strain relationship, whereas real nanocrystallineMgO may contain defects and dislocations that make this assumption less realistic. UDEDM therefore provides a more physically comprehensive description by considering the deformation energy density and anisotropic elastic modulus.The porous and agglomerated morphology observed in SEM images is associated with rapid gas release during synthesis, resulting in the formation of nanosized, nearly spherical MgO particles. These morphological observations support the crystallite size estimations obtained from the Scherrer method, Gaussian peak fitting, and various Williamson–Hall models .Overall, these results demonstrate that the CCT method is an effective approach for synthesizing structurally stable and optically active MgO nanoparticles with potential applications in various industrial and technological fields.

Acknowledgements: The authors express their sincere gratitude to the management of Bankura Zilla Saradamani Mahila Mahavidyapith and Ramananda College, Bishnupur, Bankura, India, for their continuous support and encouragement. The authors also gratefully acknowledge the Coordinator of the Centre of Excellence in Advanced Materials, National Institute of Technology, Durgapur, India, for providing the facilities and support for the microstructural characterization of the nanomaterial samples.

Conflict of interest: None

Source of support: None

REFERENCES

Ahmed, S., Rehman, H. U., Ali, Z., Qadeer, A., Haseeb, A., & Ajmal, Z. (2021). [Article title not

provided]. *Surface Interfaces, 23*, 100953. https://doi.org/10.1016/j.surfin.2021.100953

Amina, M., Al Musayeib, N. M., Alarfaj, N. A., El-Tohamy, M. F., Oraby, H. F., Al Hamoud, G. A., Bukhari, S. I., & Moubayed, N. M. S. (2020). Biogenic green synthesis of MgO nanoparticles using *Saussurea costus* biomasses for a comprehensive detection of their antimicrobial, cytotoxicity against MCF-7 breast cancer cells and photocatalysis potentials. *PLOS ONE, 15*(8), e0237567. https://doi.org/10.1371/journal.pone.0237567

Baiju, V., Devadathan, D., Rejani, P., Kumar, G. S., & Raveendran, R. (2021). Effect of annealing temperature on the purity of zinc aluminate synthesized by SCS method. *AIP Conference Proceedings, 2379*, 030014. https://doi.org/10.1063/5.0058365

Calcination temperature-dependent surface structure and physicochemical properties of magnesium oxide. (2015). *RSC Advances*. https://doi.org/10.1039/C5RA17031A

Chen, M., Zhang, Y., Xing, L., Liao, Y., Qiu, Y., Yang, S., & Li, W. (2017). [Article title not provided]. *Advanced Materials, 29*, 1607015. https://doi.org/10.1002/adma.201607015

De, S., & Bhattacharjee, B. (2025). Facile synthesis of magnesium oxide nanoparticles for effective photocatalytic degradation of dyes. *Asian Journal of Chemistry, 37*(4), 925–930. https://doi.org/10.14233/ajchem.2025.33266

Effect of calcination temperature on lattice defects in impure magnesium oxide. (1979). *Ceramurgia International, 5*(1), 45–48. https://doi.org/10.1016/0390-5519(79)90011-5

Farhadi, S., & Salehi, R. (2021). Structural, optical and magnetic properties of transition metal-doped MgO nanoparticles synthesized by a solution combustion method. *Journal of Alloys and Compounds, 851*, 156840. https://doi.org/10.1016/j.jallcom.2020.156840

Gatou, M.-A., Skylla, E., Dourou, P., Pippa, N., Gazouli, M., Lagopati, N., & Pavlatou, E. A. (2024). Magnesium oxide (MgO) nanoparticles: Synthetic strategies and biomedical applications. *Crystals, 14*(3), 215. https://doi.org/10.3390/cryst14030215

Gopinath Kasi, N., Stalin, N., Rachtanapun, P., Jantanasakulwong, K., Halder, J. N., Phongthai, S., Worajittiphon, P., Seo, J., & Thanakkasaranee, S. (2025). Effect of calcination temperatures on crystallite size, particle size, and antimicrobial activity of synthesized MgO and its cytotoxicity. *International Journal of Molecular Sciences, 26*(10), 4868. https://doi.org/10.3390/ijms26104868

Hassanzadeh-Tabrizi, S. A. (2023). Precise calculation of crystallite size of nanomaterials: A review. *Journal of Alloys and Compounds*. [Volume, page range and DOI not provided.]

Hegde, V. N., et al. (2024). Effect of calcination temperature on structural, morphological, elastic and electrical properties of MgO nanoparticles Sol–gel synthesis and comprehensive characterization of MgO nanostructures: Structural, optical, and dielectric insights. (2026). *Scientific Reports*. https://doi.org/10.1038/s41598-026-44397-5

synthesized by combustion method. *Journal of Physics and Chemistry of Solids, 192*, 112071. https://doi.org/10.1016/j.jpcs.2024.112071

Hornak, J., Trnka, P., Kadlec, P., Michal, O., Mentlík, V., Sutta, P., Csányi, P., & Tamus, G. M. (2021). Synthesis, properties, and selected technical applications of magnesium oxide nanoparticles: A review. *International Journal of Molecular Sciences, 22*(23), 12752. https://doi.org/10.3390/ijms222312752

Javed, U., Sohail, H. A., Nazneen, A., Atif, M., Mustafa, G. M., & Khan, M. I. (2024). Tuning of structural, magnetic, and optical properties of ZnO nanoparticles by Co and Cu doping. *Solid State Communications, 390*, 115616. https://doi.org/10.1016/j.ssc.2024.115616

Jensen, H., Pedersen, J. H., Jørgensen, J.-E., & Pedersen, J. S. (2006). Determination of size distributions in nanosized powders by TEM, XRD, and SAXS. *Journal of Experimental Nanoscience, 1*(3), 355–373. https://doi.org/10.1080/17458080600752482

Jintakosol, T., & Singjai, P. (2009). Effect of annealing treatment on luminescence property of MgO nanowires. *Current Applied Physics, 9*, 1288–1292. https://doi.org/10.1016/j.cap.2009.02.014

Kaneko, S., Nagano, T., Akiyama, K., Ito, T., et al. (2010). Large constriction of lattice constant in epitaxial magnesium oxide thin film: Effect of point defects on lattice constant. *Journal of Applied Physics, 107*, 073525. https://doi.org/10.1063/1.3361482

Khorsand Zak, A., Abd. W. H., Majid, W. H. A., & Yousefi, R. (2011). X-ray analysis of ZnO nanoparticles by Williamson–Hall and size-strain plot methods. *Solid State Sciences, 13*(1), 251–256. https://doi.org/10.1016/j.solidstatesciences.2010.11.024

Kumar, S. A., Jha, S. K., & Ahmad, M. K. (2022). Facile green synthesis of magnesium oxide nanoparticles using tea (*Camellia sinensis*) extract: Characterization and antibacterial activity.

Molecules, 29(18), 4299. https://doi.org/10.3390/molecules29184299

Rani, N., Chahal, S., Chauhan, A. S., Kumar, P., Shukla, R., & Singh, S. (2019). X-ray analysis of MgO nanoparticles by modified Scherrer's Williamson–Hall and size-strain method. *Materials Today: Proceedings, 12*, 543–548. https://doi.org/10.1016/j.matpr.2019.03.096

Rodenbough, P. P., et al. (2017). Lattice expansion in metal oxide nanoparticles: MgO, Co_3O_4, and Fe_3O_4. *Journal of the American Ceramic Society*. https://doi.org/10.1111/jace.14478

Shaikh, G. Y., Nilegave, D. S., Girawale, S. S., Kore, K. B., Newaskar, S. R., Sahu, S. A., & Funde, A. M. (2022). Structural, optical, photoelectrochemical, and electronic properties of the photocathode CuS and the efficient CuS/CdS heterojunction. *ACS Omega, 7*(34), 30233–30240. https://doi.org/10.1021/acsomega.2c03352

Shoeb, M., Ahmad, S., Mashkoor, F., Khan, M. N., Hasan, I., Singh, B. R., & Jeong, C. (2024). Investigating the size-dependent structural, optical, dielectric, and photocatalytic properties of benign-synthesized ZnO nanoparticles. *Journal of Physics and Chemistry of Solids, 184*, 111707. https://doi.org/10.1016/j.jpcs.2023.111707

ShunmugaSundaram, P., Sangeetha, T., Rajakarthihan, S., Vijayalakshmi, R., Elangovan, A., & Arivazhagan, G. (2020). XRD structural studies on cobalt-doped zinc oxide nanoparticles synthesized by coprecipitation method: Williamson–Hall and size-strain plot approaches. *Physica B: Condensed Matter, 595*, 412342. https://doi.org/10.1016/j.physb.2020.412342

Veerasamy, R., Xin, T. Z., Gunasagaran, S., Xiang, T. F. W., Yang, E. F. C., Jeyakumar, N., & Dhanaraj, S. A. (2011). Biosynthesis of silver nanoparticles using mangosteen leaf extract and evaluation of their antimicrobial activities. *Journal of Saudi Chemical Society, 15*(2), 113–120. https://doi.org/10.1016/j.jscs.2010.06.022

Varma, A., Mukasyan, A. S., Rogachev, A. S., & Manukyan, K. V. (2016). Solution combustion synthesis of nanoscale materials. *Chemical Reviews, 116*, 14493–14586. https://doi.org/10.1021/acs.chemrev.6b00279

Wadhwa, S., Tyagi, A., & Dixit, A. (2019). Impact of annealing on the structural properties of MgO nanoparticles by XRD analysis and Rietveld refinement. *AIP Conference Proceedings, 2093*(1), 020024. https://doi.org/10.1063/1.5090087

Wang, Y., & Wu, Z. (2008). First-principles calculations of the elastic properties of MgO under high pressure. *Physics of the Earth and Planetary Interiors, 170*(3–4), 211–215. https://doi.org/10.1016/j.pepi.2008.05.008

Wei, Q., & Lieber, C. M. (2000). Solution-based synthesis of magnesium oxide nanorods. *Materials Research Society Symposium Proceedings, 581*, 3–7. https://doi.org/10.1557/PROC-581-3